Enhanced angular overlap model for nonmetallic *f*-electron systems

Z. Gajek*
Institute of Low Temperature and Structure Research, Polish Academy of Sciences, P Nr 1410, 50-950 Wrocław 2, Poland
(Received 13 December 2004; revised manuscript received 11 April 2005; published 22 July 2005)

An efficient method of interpretation of the crystal field effect in nonmetallic *f*-electron systems, the enhanced angular overlap model (EAOM), is presented. The method is established on the ground of perturbation expansion of the effective Hamiltonian for localized electrons and first-principles calculations related to available experimental data. The series of actinide compounds AO_2, oxychalcogenides AOX, and dichalcogenides UX_2 where X=S,Se,Te and A=U,Np serve as probes of the effectiveness of the proposed method. An idea is to enhance the usual angular overlap model with *ab initio* calculations of those contributions to the crystal field potential, which cannot be represented by the usual angular overlap model (AOM). The enhancement leads to an improved fitting and makes the approach intrinsically coherent. In addition, the *ab initio* calculations of the main, AOM-consistent part of the crystal field potential allows one to fix the material-specific relations for the EAOM parameters in the effective Hamiltonian. Consequently, the electronic structure interpretation based on EAOM can be extended to systems of the lowest point symmetries or/and deficient experimental data. Several examples illustrating the promising capabilities of EAOM are given.

DOI: 10.1103/PhysRevB.72.045139 PACS number(s): 71.23.An, 71.70.Ch, 75.30.Gw

I. INTRODUCTION

The list of phenomena traditionally discussed in the context of the crystal field (CF), like optical excitations, Schottky effect, Van Vleck susceptibility, etc., has been extended in recent decades to include such intriguing and different manifestations of many-body effects as unconventional superconductivity, Kondo-like behavior, magnetic rearrangements, and non-Fermi liquids. The complexity of these phenomena contrasts with the apparent simplicity of the one-electron, local CF potential in the effective Hamiltonian. Nevertheless, its reliable determination meets serious difficulties even today, 75 years after Bethe considered the CF effect for the first time.[1] These concern not only calculations from first principles but also common phenomenological schemes based exclusively on symmetry arguments. In practice, only compounds of the highest symmetries can be handled satisfactorily. In most cases, the usual least-squares fitting of all the parameters in the effective Hamiltonian requires additional, more or less heuristic reasoning referring to physical or chemical foundations. Alternatively, simplified phenomenological models are employed to circumvent the problem of overnumerous parameters. The accuracy of these models is one of the issues the present discussion addresses. We focus on the angular overlap model (AOM) inspired by the molecular orbital theory[2,3] and confirmed by further theoretical calculations.[4,5] The AOM assumes, as in the superposition model (SPM),[6] a total CF potential in the form of a superposition of axial potentials due to ligands represented by a set of intrinsic parameters. The approximations are rather crude but the number of free parameters is remarkably reduced in comparison with basal parametrization, especially for low-symmetry systems. A more refined analysis of the experimental data, having fundamental meaning for subtle magnetic properties or cooperative phenomena at low temperatures, may require methods that are more rigorous. Can these simplified CF models be improved without increasing the number of free parameters? This question is discussed here on the grounds of *ab initio* calculations for a series of actinide compounds.

There are two general ways to determine the CF potential from first principles: one based on the perturbation theory and the idea of the effective Hamiltonian for localized, open-shell electrons[4] and a second developed on the grounds of the density functional theory (DFT).[7,8] Taking into account proximity of the band states or/and widening of the localized *nf* states, DFT seems to be a more suitable method for metallic systems. However, the early implementations of DFT based on the local spin density approximation (LSDA) failed to predict not only the subtle magnetic, low-temperature thermodynamic properties and the low-energy spectra but even some of the main characteristics of the crystals. For instance, the antiferromagnetic semiconductor UO_2 becomes a ferromagnetic metal.[9] Over the years some inherent shortcomings of the LSDA, like double counting of states or the requirement for the electron density to be a slowly varying function, were lessened or removed by various corrections: the generalized gradient approximation, U approximation, self-interaction correction, or, more recently, the hybrid density functional theory.[9] Nevertheless, these improvements, to our best knowledge, have not eliminated completely the problems related to the CF effect (see the discussion in Ref. 10, p. 206).

An alternative approach,[10,11] based on the perturbation expansion of the effective Hamiltonian, seems to be more efficient and reliable in providing material-specific details of the electronic structure. The model was developed for nonmetallic systems successively by Sugano and Schulman,[12] Newman and co-workers,[6,13] Faucher and Garcia,[14] and others (see Refs. 10 and 13, and references therein). The effective CF potential appears in this approach as a sum of several contributions, most of which obey the assumptions of the mentioned simplified phenomenological models.

In metallic systems, additional mechanisms, apart from those characteristic for insulating crystals, have to be considered:[10] mixing of the localized and band states (hy-

bridization) and static and dynamic screening of the conduction electrons including offset screening of the carriers occupying a virtual bond state. None of them can be regarded as a pure superposition of the nearest-neighbor contributions. Moreover, the role of each mechanism remains unclear; for instance, the hybridization term alone can represent almost the whole CF effect for some compounds,[15] but for others it is only one of the important contributions.[16] In addition, the dynamic correlations become increasingly important as the localized state nears the conduction band, giving rise to many-electron crystal field effects or even leading to a breakdown of the effective Hamiltonian theory for localized electrons. Thus, an extension of the crystal field theory toward self-consistent models for mixed systems of localized and itinerant electrons attracts growing attention recently.[17] However, material-specific results based on these efforts have not been achieved yet and we have to confine our discussion to simpler systems in which an admixture of the band states to the localized ones or a mixing of the states localized on adjacent atoms can be treated as an additional perturbation term in our effective Hamiltonian. We only note that there exists a subgroup of metallic systems for which the basic CF mechanisms remain essentially the same as those for ionic crystals.[18]

The accuracy of the simplified models has been discussed on the grounds of numerical simulations for actinide compounds.[5] It has turned out that the lattice contributions were not always negligible and the e_δ contribution (see Sec. II B) has not behaved as a characteristic, intrinsic parameter of the metal-ligand (M-L) interaction. Moreover, the present paper shows that the main AOM energies e_σ and e_π may also fail a more rigorous test of their transferability. Thus we propose a quasiphenomenological approach that links the simplified phenomenological model with partial *ab initio* calculations: the *enhanced angular overlap model* (EAOM).

The paper is organized as follows. The perturbation expansion leading to the effective Hamiltonian and the angular overlap model is outlined in Sec. II. Details of the *ab initio* calculations and results obtained for UX_2 (X=S,Se,Te) and those reported previously for AO_2 (Ref. 16) and AOX (Refs. 19 and 20) are discussed in Sec. III, including their reliability, adequacy of the superposition approximation, and variation of the intrinsic parameters with distance across the series. The enhanced angular overlap model is considered in Sec. IV together with examples of its application. Concluding remarks are provided in Sec. V. To ensure self-consistency of the presentation some known formulas used in the calculations are included in Appendixes.

II. FORMULATION

A. Effective Hamiltonian

Since the theoretical model applied here has been presented elsewhere (see Ref. 10 and references therein), we only recapitulate its main points for clarity of further discussion. The basic assumption of the model is that all magnetic electrons in a crystal occupy stationary orbitals, $5f$ in the case of the actinide ions discussed here. The initial infinite many-electron problem is reduced then to a single cluster consisting of a metal ion and nearest neighbors—the ligands. The outside of the cluster is represented by the classic electrostatic potential. The cluster itself is treated as a system of weakly interacting groups of electrons localized on different ions. This allows one to apply the group product function formalism and reduce the initial N-electron system to several subsystems of lower dimensions.[4,10,21] The zero-order group product wave functions are built up from the free-ion spin orbitals obtained with the standard self-consistent Dirac-Slater procedure and stabilization potential wall for anions, the depth of which is determined by the Madelung energy.[22] The function basis is restricted to the ground and the most important inter- and intraion excited electronic configurations. Projection of the initial function space onto the ground configuration subspace, contraction of the closed-shell states, and renormalization due to the nonorthogonality of the wave functions centered on different ions are the main steps in this approach. They lead to an effective Hamiltonian defined in the restricted wave-function space spanned by the single-$5f^n$-configuration states. The effective Hamiltonian contains several renormalization terms which can be regarded as a perturbation to the initial Hamiltonian. The theory may be easily verified by the experimental data because the same function basis is employed in the conventional phenomenological description of the electronic structure (see Appendix A). The nonspherical part of the effective Hamiltonian defines the effective CF potential $V(\mathbf{r})$ "seen" by a $5f$ electron. Since all the wave functions in our restricted function basis have the same radial part $(1/r)P(r)$, the Hamiltonian and all relevant operators can be contracted to the angular coordinates. The resulting operator of the CF potential $\hat{V}(\mathbf{r}/r)$ is commonly written in the form of an expansion in terms of the normalized spherical harmonics $\hat{C}_q^{(k)}$,[23]

$$\hat{V}(\mathbf{r}/r) = \sum_{k,q} B_{kq} \hat{C}_q^{(k)}(\mathbf{r}/r), \tag{1}$$

where k=2,4,6 denotes the rank of the spherical harmonic and $q=-k,-k+1,\ldots,k$ runs over its components. B_{kq} are the integrals[19]

$$B_{kq} = \int \left(\frac{1}{r} P_{nf}(r)\right)^2 V(\mathbf{r}) \hat{C}_q^{(k)*}(\mathbf{r}/r) d\mathbf{r}, \tag{2}$$

playing the role of adjustable CF parameters in the phenomenological theory.

B. Angular overlap model

The angular overlap model is a simplified phenomenological approach based on certain restrictive assumptions, inspired by the Hückel molecular orbital model.[2,3] From among various formulations appearing in the literature we chose one proposed by Schäffer[24] which does not refer to the molecular orbital scheme. This formulation is consistent with the perturbation approach outlined above and the Newman superposition model[6] discussed later. According to it, the CF potential V is a superposition of independent contributions—the potentials v_t generated by the nearest-neighbor ligands:

$$V(\mathbf{r}) \simeq \sum_t v_t(\mathbf{r}-\mathbf{R}_t), \tag{3}$$

where $\mathbf{R}_t$ denotes the position of the tth ligand. Additionally, as an approximation, the local symmetry of the separated metal-ligand system is assumed to be axial.

The AOM parameter e_μ^t of the given ligand t is defined as a matrix element of the ligand potential v_t in the coordinate system t with the z axis along the metal-ligand *t-linear ligator* in which v_t is diagonal:

$$e_\mu^t \equiv e_\mu^t(R_t) = \langle \pm\mu|v_t|\pm\mu\rangle_t, \tag{4}$$

where the index $\mu=0(\sigma),1(\pi),2(\delta),3(\phi)$denotes the absolute value of the magnetic quantum number of the $5f$ electron. It is convenient to fix the energy scale by setting $e_\phi=0$. In practice we put $\tilde{e}_\mu \equiv e_\mu - e_\phi$ instead of e_μ. Since only $\tilde{e}_\mu$'s are used hereafter, we omit the tilde for convenience. Transformation properties under the *rotation group* R_3 of the $l=3$ wave functions allow one to express the matrix elements of V in the global coordinate system in terms of e_μ^t's:

$$\langle m|V|m'\rangle = \sum_t \sum_\mu D^{(3)*}_{\mu m}(0,\Theta_t,\Phi_t) D^{(3)}_{\mu m'},(0,\Theta_t,\Phi_t) e_\mu^t, \tag{5}$$

where $D^{(3)}_{\mu m}(0,\Theta_t,\Phi_t)$ is the matrix element of the irreducible representation $D^{(3)}$ of the rotation group and R_t,Θ_t,Φ_t are the angular (global) coordinates of the ligand t. Equation (5) is the fundamental equation of the AOM. It relates the matrix elements of the CF potential to the intrinsic parameters describing the individual metal-ligand pairs through rotation matrices dependent on the geometry of the coordination polyhedron.

For practical purposes it is advisable to relate the AOM parameters to the basic CF parameters B_{kq}. Comparing the right side of Eq. (5) with the matrix elements of the potential given by the expansion (1) and using the properties of tensor operators and the rotation matrices[25,26] we obtain after some manipulation the following relation:

$$B_{kq} = \sum_\mu W^\mu_{kq} e_\mu \tag{6}$$

where

$$W^\mu_{kq} = \frac{2k+1}{7}\left[\begin{pmatrix} 3 & k & 3 \\ 0 & 0 & 0 \end{pmatrix}\right]^{-1} (-1)^\mu (2-\delta_{\mu 0}) \times \begin{pmatrix} 3 & k & 3 \\ -\mu & 0 & \mu \end{pmatrix} \sum_t C^{(k)*}_q(\Theta_t,\Phi_t) s^t_\mu, \tag{7}$$

$$s^t_\mu = \frac{e^t_\mu}{e_\mu}, \tag{8}$$

and (:::) are the $3j$ symbols. The e_μ parameters are the mean values of the AOM parameters averaged over t. Their introduction into Eq. (6) is one of the possible solutions of the problem of several sets of intrinsic parameters in the case of nonequivalent ligands. Note that if W^μ_{kq} and s^t_μ given by Eqs. (7) and (8) are inserted into Eq. (6), then the averaged e_μ's cancel out. Moreover, the ratios s^t_μ can be treated as parameters of the model instead of e^t_μ's. From the algebraic point of view, this is only a scaling of the parameters without loss of generality. In practice, it is possible to estimate the ratios independently (this question is discussed later) and to consider the averaged quantities e_μ to be adjustable parameters. The W^μ_{kq} coefficients absorb all information about the geometry of the coordination polyhedron whereas the ratios s^t_μ encode differences in the AOM parameters due to the individual M-L_t distances. The distance dependence of s^t_μ has exponential character,[5] yet, within a limited range of distances, it is fairly well approximated by the simple power function

$$s^t_\mu = \left(\frac{R}{R_t}\right)^{\alpha_\mu} \tag{9}$$

with the power exponents α_μ taking values in the range 4.3 to 8.9 in the case of actinide ions and simple ligands.[5,10,19]

An extension of the above equations to arbitrary number of different anions is straightforward. Note that the partitioning (3) neglects the contribution from the outside of the coordination cluster. This contribution and also other effects, which cannot be represented in the form of the decomposition (3), are included explicitly in the enhanced model presented below.

The AOM reduces the number of adjustable parameters describing the CF effect to 3. The strength of the model stems from the fact that the local interion interaction parameters e_μ may be regarded as quantities characteristic for a given metal-ligand (M-L_t) pair. They allow one to verify unphysical solutions generated by false minima of the fitting procedures in the standard parametric analysis on the one hand and to indicate the ensuing approximations in the case of especially complex systems on the other. Due to the dominant character of the renormalization terms [see Sec. II C and Eq. (14)], the AOM parameters e_σ and e_π manifest several characteristic properties:[4,5,10,13,19,27] (i) their values reflect the spectrochemical ordering of the anions; and (ii) decrease slightly with increasing atomic number along the lanthanide and actinide series and, independently, with decreasing oxidation number of the metal ion; (iii) $e_\sigma > e_\pi > |e_\delta|$; (iv) $e^t_\mu / e^{t'}_\mu \approx$ const for two different M-L_t and M-$L_{t'}$ systems ($t \neq t'$); (v) $e^t_\pi / e^t_\sigma \approx$ const for a given M-L_t pair; (vi) the e_δ parameter, usually of minor importance, has been shown to be "lattice sensitive"[5] if obtained from the fitting of the experimental data. For this reason, transferability of e_δ between various compounds seems to be questionable in the conventional AOM.

Even though exceptions from the above rules happen (see the next section), they may serve as an instructive test of any set of CF parameters determined from the experimental data. This concerns not only the fitting results obtained with other approximate models but also the basic B_{kq} parameters, which can be "translated" to e_μ using Eq. (6) and a standard least-squares procedure.

As mentioned, one of the most widely applied approximate methods, the Newman superposition model,[6,13] is based on the same assumptions as the AOM. However, the role of intrinsic parameters is played by the B_{kq} parameters for a separated linear ligator in a local coordinate system. Due to

the assumed cylindrical symmetry of each M-L subsystem, only the parameters with $q=0$ are effective. They are denoted hereafter as "b_k" to distinguish them from the B_{k0} parameters in the global coordinate system. The relation between the two sets of intrinsic parameters, for the AOM and SPM, can be easily obtained from Eqs. (6)–(8) by rewriting them for the specific case of the separated linear ligator:

$$b_k = \frac{2k+1}{7}\left[\begin{pmatrix} 3 & k & 3 \\ 0 & 0 & 0 \end{pmatrix}\right]^{-1} \sum_{\mu=0}^{3} (-1)^{\mu}(2-\delta_{\mu 0}) \times \begin{pmatrix} 3 & k & 3 \\ -\mu & 0 & \mu \end{pmatrix} e_{\mu}. \quad (10)$$

The algebraic equivalence of the two sets of intrinsic parameters evidenced by the above relation allows one to extend the literature data for their values, independently of the way in which they have been obtained.

C. Contributions to the CF potential

The procedure outlined in Sec. II A leads to several characteristic contributions to the CF potential V, corresponding to different mechanisms. Their discussion in next sections precedes a formulation of the enhanced angular overlap model. Thus, it is advisable to separate out those that obey the assumptions of the angular overlap model (the *AOM-consistent* contributions), V^{AOM}, and the *residuum* V^{res}:

$$V = V^{AOM} + V^{res}. \quad (11)$$

In V^{AOM} one can further distinguish the *primary* (V^{pr}) and *renormalization* (V^{ren}) components:

$$V^{AOM} = V^{pr} + V^{ren}. \quad (12)$$

V^{pr} represents the Coulomb interaction (direct and exchange) of the ligand electrons, and the potential of the nuclei. It diverges from the point-charge model[1] (*pcm*) due to the charge penetration[28] (*cp*) and interionic exchange[29] (*ex*) effects included in V^{pr}:

$$V^{pr} = V^{pcm} + V^{cp} + V^{ex} + V^{prsh}. \quad (13)$$

The intraionic excitations on the metal ion induced by the primary contribution lead to the AOM-consistent part of the shielding potential V^{prsh}.

V^{ren} comprises the main renormalization terms implied by the ligand-metal charge transfer excitations—the covalency contribution V^{co},[6] and nonorthogonality of the free-ion wave functions localized on adjacent ions: the overlap contribution V^{ov},[6] and the contact shielding, V^{cs},[11]

$$V^{ren} = V^{ov} + V^{cs} + V^{co}. \quad (14)$$

V^{res} includes all the remaining terms. One can distinguish V^{nnpol}, the contribution of electric multipoles induced on ligands (polarization of nearest neighbors), V^{fn}, the electrostatic potential of the point charges and electric multipoles induced on the all the ions outside the cluster (electrostatic potential of further neighbors), and V^{ressh} which symbolizes the shielding correction to these electrostatic potentials:

$$V^{res} = V^{nnpol} + V^{fn} + V^{ressh}. \quad (15)$$

Due to the cancellation of various terms in the primary and residual contributions, V^{ren} or V^{ov} in essence turns out to be the most important mechanism for the ionic compounds in favor of the AOM.[5,6,10,13,27] This corollary is supported also by the results presented in the next section.

Explicit formulas for all the above contributions are given in Appendix B.

III. *AB INITIO* CALCULATIONS

A. Details of the calculations

The compounds under consideration represent a variety of crystal structures. The point symmetry of the metal ion varies from cubic in UO_2 (CaF_2 structure, space group $Fm3m$, 225), through D_{2d} in UOX (PbFCl-type structure, $P4/nmm$, 129),[30] C_{2v} in UTe_2 (orthorhombic space group $Immm$, 71),[31] up to C_s in β-US_2 and β-USe_2 ($PbCl_2$-type structure, $Pnma$, 62).[32]

Zero-order free-ion wave functions have been generated using the self-consistent Dirac-Slater procedure ATOM,[33,34] with the stabilizing potential well determined by the Madelung energy.[22] The calculations have been performed in the crystallographic coordinate system. The lattice sums of static and induced multipoles generated by the set of the crystal electrostatic equilibrium equations (B13) in Appendix B have been calculated according to Eq. (B12) using a modified version of the program CHLOE,[14,35] and multipole polarizabilities from Ref. 36. The summation in the multipole expansion (B12) was limited to monopoles, dipoles, and quadrupoles ($n=0,1,2$) in the present calculations. The effect of the outer electrons occupying the 6s and 6p closed shells of the metal ion has been estimated via Sternheimer's shielding factors σ_k scaling the corresponding B_{kq}'s.[37,38] The charge penetration, exchange, and renormalization terms have been calculated using the program LF developed for the f-electron compounds.[39]

The free-ion part of the effective Hamiltonian contains the intraionic Coulomb repulsion of the 5f electrons of the U^{4+} ion, controlled by the Slater integrals F^k, $k=2,4,6$, spin-orbit coupling with the ζ_{5f} parameter and further corrections of higher order (see Appendix A). The "free-ion" parameters depend on the crystal, in which the metal ion is embedded, and may vary in certain range, modifying the interterm spacing.[40] Fortunately, these differences are limited and they have rather negligible impact on the splitting of the ground multiplet. Thus, we adopt the values obtained earlier from the fitting of the optical spectra for U^{4+} in $ThGeO_4$ (in meV):[41] $F^2=5339$, $F^4=4833$, $F^6=3018$, $\alpha=3.72$, $\beta=-81.8$, $\gamma=148.8$, $M^0=0.124$, $M^2=0.069$, $M^4=0.047$, $P^2=62.0$, $P^4=31.0$, $P^6=6.2$, and $\zeta_{5f}=224.2$. The calculations of the eigenvalues and eigenvectors and/or fitting of the measured energies of electronic transitions have been performed with a set of f-shell empirical computer programs developed by Reid,[42] supplemented with a subprogram[39] POD for calculation of some thermodynamic quantities.

B. Reliability of the results

This type of *ab initio* calculation was performed previously for, among others, UO_2 and UOS,[19,20,43] compounds

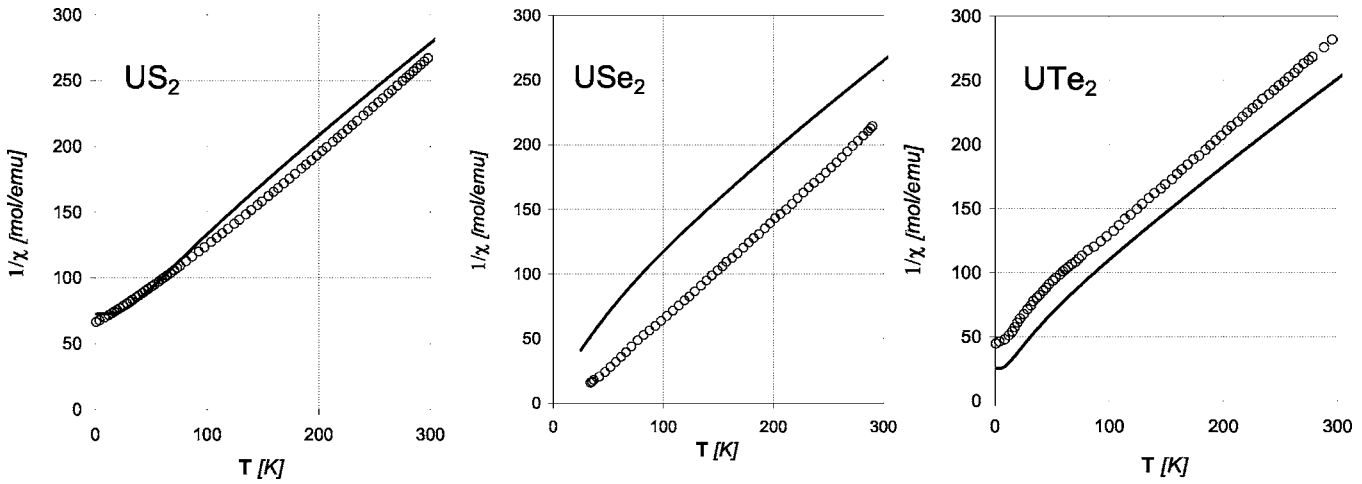

FIG. 1. Reciprocal magnetic susceptibilities of powdered dichalcogenides as a function of the temperature: comparison of the experimental (open circles) (Refs. 32, 46, and 47) and theoretical (continuous lines) curves obtained using the Van Vleck formula (C1).

for which comprehensive experimental data are available, including optical and/or inelastic neutron scattering (INS) spectra.[43–45] The discrepancy of the obtained theoretical B_{kq} parameters and the phenomenological values determined by a fitting to the experimental data did not exceed 20–30 %. Now the calculations are extended to the UX_2 subseries. For these compounds the published experimental results are not so rich.[32,46,47] We can reproduce certain thermodynamic averages, e.g., the paramagnetic Van Vleck susceptibility (see Appendix C) depicted in Fig. 1. The corresponding energy levels are shown in Fig. 2 and they are discussed later. The experimental slope, shape, and variation of the temperature-independent susceptibility at the lowest temperatures along the series agree quite well with the results of the *ab initio* calculations. A discrepancy between the theoretical and experimental lines visible for USe_2 and UTe_2 can be attributed to the interionic exchange not included in the model calculations. Judging from the mutual shifts of the lines, the interaction has to be of ferromagnetic type for USe_2 and greater in the absolute value than the antiferromagnetic type observed for UTe_2. The first excited level lying at 8.0, 1.6, and 2.5 meV for the U^{4+} ion in US_2, USe_2, and UTe_2, respectively (see Fig. 2) influences the magnetic properties of these systems with a singlet ground state. Above 20 K, UTe_2 and especially USe_2 behave as if they had a degenerate ground state. The relatively weak U-U exchange interaction in USe_2 (U-U distance[32] of 0.423 nm) turns out to be sufficient to induce long-range ferromagnetic order below 14 K.[46] Note that the first excited state has the lowest energy just for this compound. USe_2 is the only dichalcogenide that orders magnetically.[32] The lack of ordering in UTe_2 with the shortest U-U distance 0.378 nm may be due to the fact that only one of seven neighboring uranium ions is placed at that distance, whereas four are placed at 0.490 nm and two at 0.416 nm. A different curvature of the theoretical and experimental reciprocal susceptibilities observed for USe_2 below 60 K may be ascribed to the magnetic fluctuations increasing with temperature approaching the critical point, which were not taken into account in the model calculations. The effective magnetic moments, of $2.94\mu_B$, $3.01\mu_B$, and $3.09\mu_B$, are lower than those derived from the experimental curves, $3.25\mu_B$, $3.20\mu_B$, and $3.21\mu_B$, reported for US_2, USe_2,[46] and UTe_2,[47] respectively.

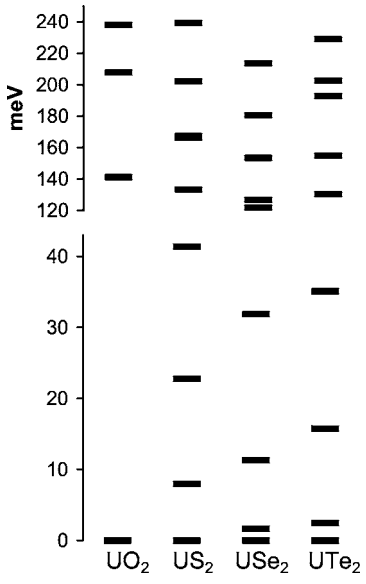

FIG. 2. Splitting of the uranium (4+) ground term $^3H_4$ in UX_2 crystals obtained by simultaneous diagonalization of Hamiltonian (A1),(A2) with the CF parameters determined from first principles. The lower part of the diagram uses a scale enlarged several times as compared with that for the upper part.

Figure 2 shows the splitting of the ground term $^3H_4$ of the $U^{4+}(5f^2)$ ion in the UX_2 series, obtained by simultaneous diagonalization of the Hamiltonian (A1),(A2), with the CF parameters determined from first principles shown in Table I and the free-ion parameters listed above.These results have been employed in calculations of the temperature dependencies of the magnetic susceptibilities discussed above. The B_{kq} parameters in Table I reveal no regularity along the series which might be expected, for instance, from the spectrochemical ordering of ligands. This observation seems not to be only a consequence of the inherent ambiguity of the CF parametrization (CFP) in low-symmetry systems[48] since it would be difficult to find any trend also in the energy levels

TABLE I. AOM-consistent (12) and residual (15) contributions to the CF parameters calculated from first principles for the UX_2 series in the crystallographic coordinate systems (Ref. 50). The primary contribution V^{pr} (13), renormalization term V^{ren} (14), ligand polarization $V^{mn\,pol}$ (B12), and potential of the further neighbors V^{fn} are specified for USe_2 in parentheses. All values in meV.

	US_2			USe_2				UTe_2		
	V^{AOM}	V^{res}	V	V^{AOM}	$(=V^{ren}+V^{pr})$	V^{res}	$(=V^{mn\,pol}+V^{fn})$	V	V^{AOM}	V^{res}	V
B_{20}	65	−17	48	84	(73+11)	−10	(−24+14)	74	38	13	51
B_{21}	−203	−3	−206	−200	(−194−5)	−6	(−1−5)	−206			
B_{22}	−79	−6	−85	−24	(−26+3)	−3	(−9+6)	−26	28	42	70
B_{40}	−88	2	−86	−71	(−52−19)	4	(4−0)	−67	−436	−184	−619
B_{41}	82	6	88	39	(32+7)	−5	(0−5)	34			
B_{42}	−274	−8	−282	−264	(−297+33)	−16	(6−22)	−280	364	79	442
B_{43}	257	45	301	186	(236−49)	26	(25+1)	212			
B_{44}	−60	−51	−111	−64	(−62−2)	−48	(−21−27)	−112	74	−26	48
B_{60}	174	−2	172	78	(80−3)	1	(2−1)	78	87	4	91
B_{61}	−233	−1	−233	−230	(−311+82)	−1	(−1+0)	−231			
B_{62}	394	5	398	340	(441−101)	3	(−5+9)	344	11	−6	6
B_{63}	171	−1	170	203	(248−45)	−1	(−1−0)	202			
B_{64}	37	18	55	34	(59−26)	9	(8+1)	43	−122	26	−96
B_{65}	−369	−10	−379	−320	(−383+63)	−4	(−4−0)	−324			
B_{66}	243	9	252	212	(262−50)	6	(2+4)	219	−151	0	−151

shown in Fig. 2. Analogous behavior of the *AOX* series has been ascribed to the influence of the competing oxygen and chalcogenide groups in the W_{kq}^{μ} coefficients (7).[19,20] Now it becomes evident that also in the case of one type of anion the coordination geometry may obscure the expected regularities so clearly manifested, on the other hand, by the intrinsic AOM parameters (cf. Table II). As we see in the next section, possible trends in CFP sets revealed elsewhere using an independent method based on certain conserved quantities associated with CF parameters[49] may be governed by the AOM-consistent part of the crystal field.

C. AOM-consistent part of crystal field

The results displayed in Table I are indicative of the essential meaning of the AOM-consistent contributions. Nevertheless, they also show that the residual contribution may become crucial for some parameters as in the case of B_{44} for US_2 or B_{22} for UTe_2. More detailed data, which are presented in Table I for USe_2, give some idea about the role of the particular CF mechanisms. Mutual compensation of the various primary components and the importance of the renormalization terms is clearly manifested there.

Handling each nonequivalent *M-L* pair independently in compounds like US_2 (with six different M-L_t distances and two nonequivalent crystallographic positions of the sulfur ion) would multiply the number of intrinsic parameters, making the model practically intractable. Usually, the dependence of the intrinsic parameters e_{μ} [or their renormalized counterparts s_{μ} (8)] on the *M-L* distance R is assumed to have a definite character.[13,19] In a limited range of distances around an average value for a given *M-L* bond, it is approximated by the power function (9). The power exponents α_{μ} are treated then as an additional characteristic of the *M-L* bond that allows one to maintain the minimal number of independent parameters.

The simulations of the $e_{\mu}(R)$ functions have been performed for all the uranium linear ligators occurring in the series U^{4+}-X^{2-}. As Eqs. (B4)–(B10) in Appendix B show, the functions are determined by squares of metal-ligand overlap integrals and Madelung energies of the ions in crystals. To ensure comparability of the results obtained for different *ML* pairs, a virtual ML_2 crystal of the CaF_2 structure has been employed, where ligands form a cube with its center occupied by the metal ion. The Madelung potential at the *L* and *M* sites in this structure is given by the formulas $U^L=-8.14e/a$ and $U^M=15.13e/a$, respectively, whereas the lattice constant a is related to the *M-L* distance R by the expression $R=\sqrt{3}a/4$. The intrinsic parameters depend on U^L and U^M in a nontrivial way through the zero-order wave functions and explicitly due to the renormalization terms (B4) and (B6). This implies the use of different free-ion wave functions for each R. The calculations have been performed for seven values of R distributed uniformly between 0.18 and 0.40 nm. The radius D of the stabilizing potential well for the negative ions of the U^L depth has been assumed to be equal to $-2e/U^L$.

The results are shown in Fig. 3. Due to the predominating renormalization terms (cf. Fig. 4), the $e_{\mu}(R)$ functions have an exponential character for *M-L* distances around the average values. For larger distances, where the electrostatic contributions dominate, they take the form of a polynomial. The slope of $e_{\sigma}(R)$ decreases in the limit of short distances, more visibly on going from the oxide to the telluride. The function $e_{\sigma}(R)$ reaches a maximum for the U^{4+}-Te^{2-} bond. Figure 4 indicates that the importance of the charge penetration rapidly increases as compared with that for other mechanisms. Since this contribution has opposite sign for e_{σ} and e_{π}, the

TABLE II. Results of *ab initio* calculations of the AOM parameters (in meV) corresponding to the AOM-consistent part of the CF potential for various A^{4+}-X^{2-} systems and the average interion distances R_{av}.

	R_{av} (nm)	e_σ	e_π	e_δ
U^{4+}-O^{2-} in				
UO_2	0.237	350	209	64
UOS[a]	0.234	340	211	63
UOSe[a]	0.236	324	196	55
UOTe[a]	0.237	316	186	46
U^{4+}-S^{2-} in				
UOS	0.293	211	96	32
US_2	0.289	265	102	36
U^{4+}-Se^{2-} in				
UOSe	0.304	204	91	31
USe_2	0.301	240	88	30
U^{4+}-Te^{2-} in				
UOTe	0.325	185	90	31
UTe_2	0.317	190	88	29
Np^{4+}-O^{2-} in				
NpO_2	0.235	317	186	56
NpOS	0.233	304	181	53
NpOSe	0.235	291	169	47
Np^{4+}-S^{2-} in				
NpOS	0.291	191	87	30
Np^{4+}-Se^{2-} in				
NpOSe	0.302	183	82	29

[a]From Ref. 19.

ratio e_π/e_σ increases in the limit of small distances.

A similar behavior, although not so evident, can be deduced from the data presented in Table II of Ref. 51 for Pr^{3+}-Cl^-, if the Coulomb contributions are scaled using the Sternheimer shielding factors and the SPM parameters are converted into the AOM ones by Eq. (10). An open question is whether the observed increase of the e_π/e_σ ratio at the lowest distances characteristic for dense systems is a true property of metals. We only note that analogous distance dependencies of the AOM parameters for the Sm^{2+}-Cl^- and Sm^{2+}-F^- systems derived from the data reported in Ref. 52 did not confirm this conjecture.

The model calculations taking into account the variation of Madelung energy with the *M-L* distance lead to lower values of the power exponents α_μ as compared with earlier estimations.[19] The AOM parameters determined for the actual crystals *AOX* and AX_2 are listed in Table II and shown in Fig. 3. Each *M-L* distance occurring in these compounds is represented in Fig. 3 by three points corresponding to the e_σ, e_π, and e_δ parameters. We see that they do not follow the smooth curves discussed above. Moreover, the crucial e_σ parameter turns out to be simultaneously the most irregular one. This is because it is especially sensitive to the variation of the Madelung potential. In light of the present calculations, the properties (i)–(v) of the AOM parameters specified in Sec. II B should be treated very carefully, not only because of the very existence of the residual contributions but also because of the just revealed inherent irregularity of the AOM-consistent contributions.

IV. ENHANCED ANGULAR OVERLAP MODEL

A. Formulation

In view of the apparent irregularity of the AOM parameters and the erratic behavior of the residual contribution (15) discussed in the preceding section and manifested in Fig. 3 and Table I, we propose to link the phenomenological AOM approach with the *ab initio* calculations in the enhanced angular overlap model. Our model assumes each ordinary CF parameter to be composed of two components: the main, adjustable one, parametrized according to Eqs. (6)–(8) and the fixed residuum B_{kq}^{res} corresponding to the potential (15), determined from Eq. (B12):

$$B_{kq} = \sum_\mu W_{kq}^\mu e_\mu + B_{kq}^{res} \tag{16}$$

with e_μ playing the role of the phenomenological EAOM parameters. The separation of the residual, off-AOM contribution from the global CF parameters allows one to establish a more precise and consistent AOM parametrization of the remainder. Consequently, the intrinsic character of the corresponding EAOM parameters is genuinely maintained. EAOM is not much more complicated than the parental AOM but the main inherent shortcoming of the latter is removed by excluding explicitly the off-AOM contributions from the simplified phenomenological treatment. These off-AOM contributions are estimated in our model from first principles. Note that its very construction makes the model

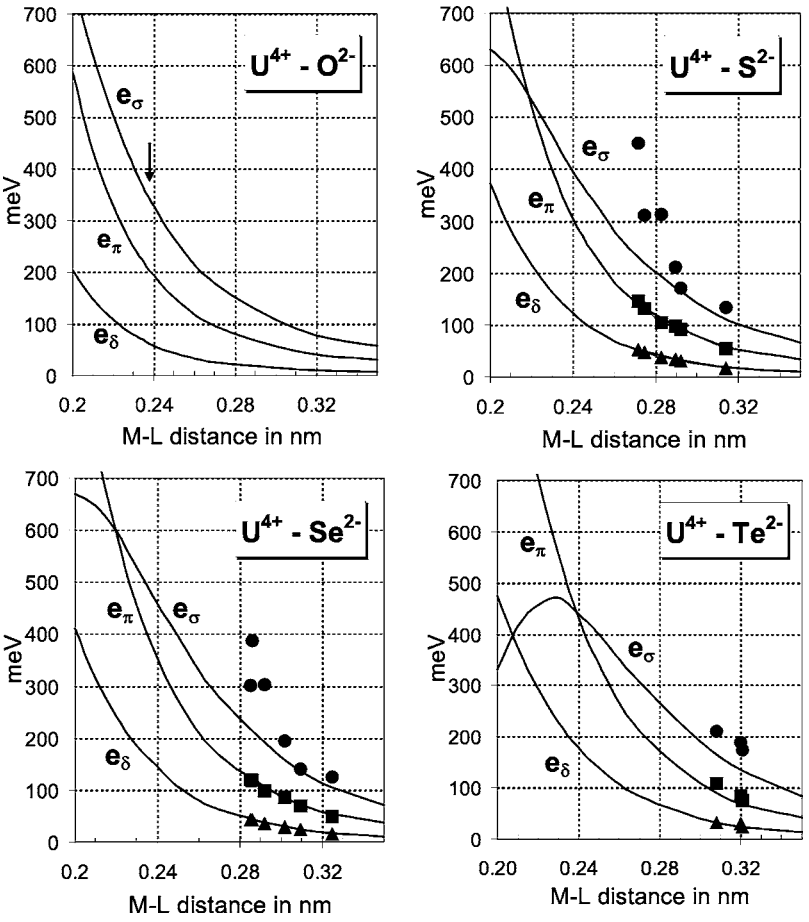

FIG. 3. Dependence of the interion effective interaction parameters of the angular overlap model on the metal-ligand distance for the U^{4+}-X^{2-} pairs in a hypothetical crystal of CaF_2 structure. The circles, squares, and triangles represent actual intrinsic parameters e_σ, e_π, and e_δ obtained for UX_2.

exact (at least in the framework of the one-electron approximation) provided the off-AOM contributions are determined precisely, which, of course, is hardly possible.

The AOM-consistent contributions listed in Table II can be regarded as a crude theoretical estimation of the EAOM parameters. Their more accurate determination requires an involved self-consistent approach to account for the energy-dependent parameter-renormalization terms.[4] Thus, treating this part of the CF potential as a phenomenological quantity allows one to handle these self-energy effects in the simplest possible way.

Naturally, the EAOM parameters obtained from the fitting of the observed electronic energy levels cannot have the same values as the AOM parameters derrived from the analo-

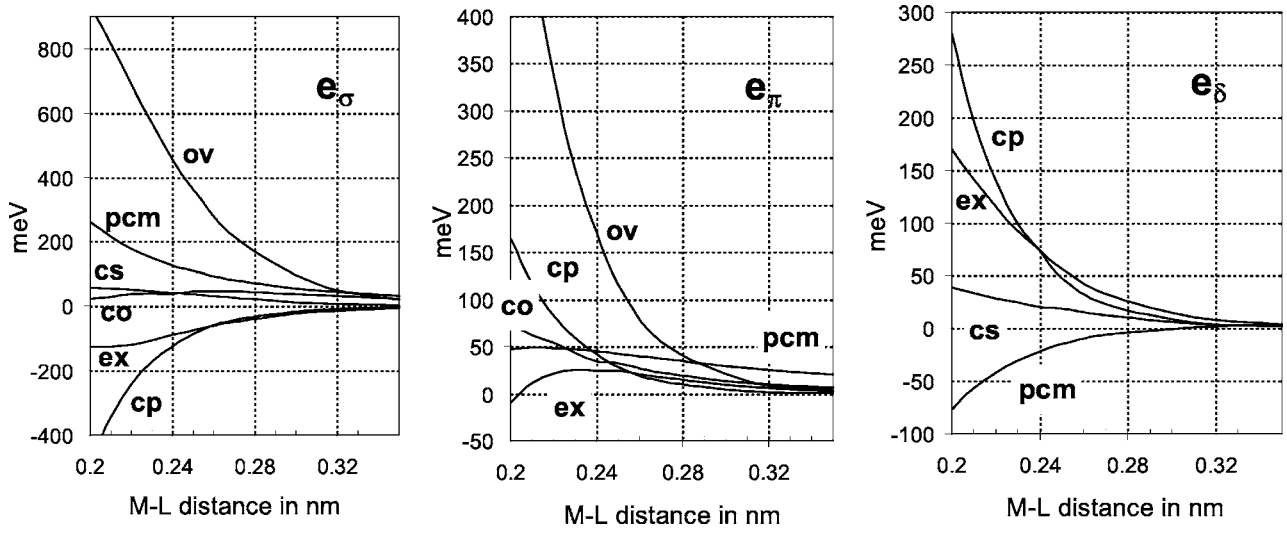

FIG. 4. Distance dependence of the main contributions to the e_μ parameters: point charges (*pcm*), overlap (*ov*), covalency (*co*), charge penetration (*cp*), exchange (*ex*), and contact shielding (*cs*).

gous fitting within the conventional AOM approach. Moreover, the rules (i)–(v) observed for the usual AOM parameters (see Sec. II B) seem more justifiable in the case of the theoretical, AOM-consistent contributions and thus, also for the EAOM parameters. Nevertheless, in light of the calculations presented in Sec. III C, still they remain acceptable in a rather limited range of the *M-L* distances, in the vicinity of their averaged values.

Compounds containing several groups of symmetry-equivalent ligands require the s_μ^t ratios in the geometrical coefficients W_{kq}^μ (7) to be determined. The observed above (see Sec. III C and Fig. 3) irregularity of the EAOM parameters due to, among others, the Madelung energy, can be reproduced by employing the *ab initio* values of these ratios. Thus, it is advisable to calculate the s_μ^t's for each individual M-L_t pair rather than applying the approximation (9).

The same theoretical calculations may also be employed to formulate further, more restrictive parametrizations, which may be helpful in the case of the most complicated experimental data. For instance, fixing both the ratios

$$s_{\mu\sigma} = e_\mu / e_\sigma, \quad \mu = \pi, \delta \tag{17}$$

equal to their theoretical values leads to a single-parameter version of the model:

$$B_{kq} = B_{kq}^{res} + \tilde{W}_{kq}\tilde{e} \tag{18}$$

with

$$\tilde{W}_{kq} = \frac{2k+1}{7}\left[\begin{pmatrix} 3 & k & 3 \\ 0 & 0 & 0 \end{pmatrix}\right]^{-1} \sum_\mu (-1)^\mu (2-\delta_{\mu 0}) \times \begin{pmatrix} 3 & k & 3 \\ -\mu & 0 & \mu \end{pmatrix} \sum_t C_q^{(k)*}(\Theta_t, \Phi_t) s_\mu^t s_{\mu\sigma}. \tag{19}$$

The $\tilde{e}$ parameter in Eq. (18) corresponds directly to e_σ but also the e_π and e_δ contributions enter into the model through the $s_{\mu\sigma}$ ratios in the above $\tilde{W}_{kq}$ coefficients. Hence, a variation of $\tilde{e}$ modifies also the e_π and e_δ contributions to the crystal field in proportions given by $s_{\mu\sigma}$. Note that Eq. (18) without the residual part would be a simple scaling of the crystal field effect predicted by the AOM-consistent part of the *ab initio* calculations.

An intermediate, two-parameter version of the model can be defined in several ways by fixing any of the $s_{\mu\sigma}$ ratios or their combinations. These single- and two-parameter versions should not be confused with models commonly employed for the transition elements[4,13] which omit simply the π and δ contributions or only the δ contribution.

Generalization of the model and Eqs. (16)–(19) to systems containing different ligands is straightforward (see the example given below).

B. Applications

Due to the highly reduced number of free parameters [up to the single-parameter version, Eq. (18)], the simplified EAOM parametrizations of the CF effect may be especially helpful in all those cases of incomplete or more complicated experimental data so frequently met in the most interesting *f*-electron systems. Three possible types of applications of EAOM are exemplified in what follows.

The first one, already discussed in Ref. 20, concerns interpretation of certain magnetic properties of NpO*X* where *X*=O, S, and Se. The procedure might be seen as a general method of interpretation of the electronic properties based on transferability of the intrinsic parameters between different compounds. The interpretation follows the phenomenological CF parameters for the specimens assumed to be known, i.e., the compounds, the electronic structure of which is believed to be reliably determined. In the example under consideration, the parameters $(B_{kq})^{\mathrm{U}}$ reported for UO_2, UO*X*, the ones of the most widely investigated uranium compounds, were employed.[19,43] The corresponding AOM parameters e_μ^{UO} and e_μ^{UX} were determined from the system of equations (16) and its version adapted to two different ligands, oxygen and chalcogenide,

$$B_{kq} = B_{kq}^{res} + \sum_\mu (W_{kq}^{\mu,\mathrm{O}} e_\mu^{\mathrm{O}} + W_{kq}^{\mu,X} e_\mu^X), \tag{20}$$

exploiting the *ab initio* values of the s_μ^t ratios. In the second phase, the procedure was reversed to estimate unknown CFP's for the less explored experimentally neptunium oxychalcogenides. First, the e_μ^{NpO} and $e_\mu^{\mathrm{Np}X}$ parameters were derived by scaling their uranium counterparts in terms of the ratios of the corresponding theoretical values: $(e_\mu^{\mathrm{Np}X}/e_\mu^{\mathrm{U}X})_{calc}$. The B_{kq}^{Np} parameters obtained, again, from Eqs. (16) and (20) were, in the final step, adjusted to match the experimental values of the ordered magnetic moments. In this phase, a simultaneous diagonalization included, apart from the CF Hamiltonian and the free-ion interactions, the intermetallic exchange interaction in the zero-temperature mean-field approximation. The magnetic properties of the neptunium oxychalcogenides, including the anisotropic ground-state magnetic moment, the temperature dependencies of the paramagnetic susceptibility and the magnetization at 0 K, were described satisfactorily in the outlined approach (see Ref. 20 for further details). The example illustrates the efficiency of the method based on the EAOM in prediction of the electronic structure in the case of inconclusive experimental data. The intrinsic parameters collected in Table II may serve as a tentative source of the relations between them in further applications of the EAOM approach.

The second example concerns interpretation of the thermodynamic and magnetic properties[53,54] and inelastic neutron scattering spectra of UOS.[45,55] In the analysis of the experimental data,[19] the initial energy level assignment was deduced on the grounds of first-principles calculations. The fitting of the INS data[45,55] was performed in two steps. First, the AOM was applied to obtain the identified INS transition energies. Subsequent refinement of the corresponding usual CF parameters yielded agreement with the remaining experimental data.[45,53,54] Special attention was paid to the ordered magnetic moment μ_{ord} and relative intensities of the INS transitions. However, the problem with the infinite number of acceptable solutions could not be resolved; namely, the experimental data for this tetragonal C_{4v} system could be satisfactory reproduced with any value of the B_{20} in the range of −50 to −223 meV, provided the remaining parameters

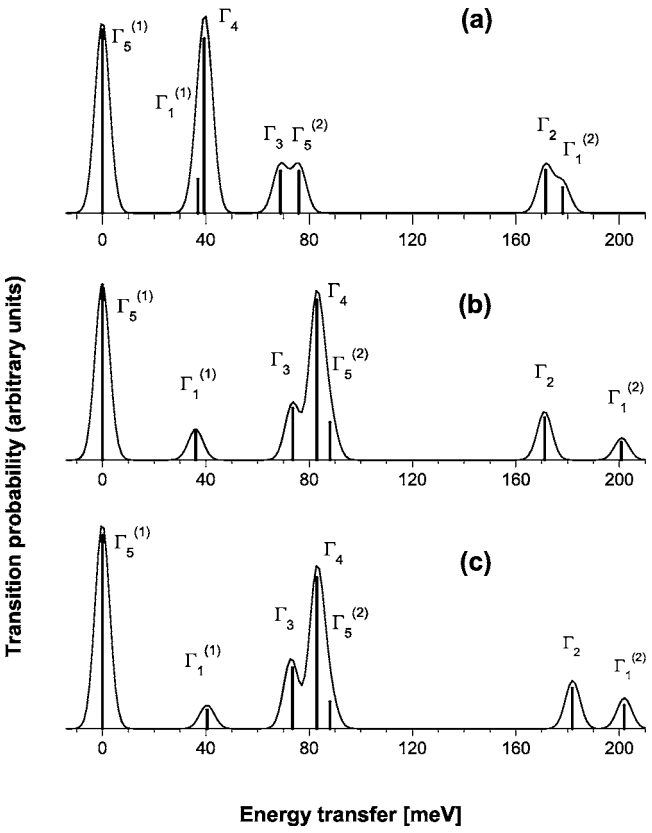

FIG. 5. Simulation of the INS spectra of UOS in various crystal field models: (a) *ab initio* calculations, (b) refined model from Ref. 19, and (c) EAOM.

B_{40}, B_{44}, B_{60}, and B_{64} were simultaneously adjusted to the given B_{20}. Some features of the electronic structure were varying with the CF parameters in this ambiguity range but they were not detectable in μ_{ord} and in the position and shape of the most intense INS lines below 100 meV. In addition, it was demonstrated[19] that the INS excitations to two of the highest levels of the $^3H_4$ term, Γ^2 and $\Gamma^{1(2)}$, could be invisible if B_{20} had decreased below −146 meV under actual incident neutron energy and angle, just as it was observed. Eventually, the set of B_{kq} parameters corresponding to the threshold value of $B_{20}=-146$ meV was accepted as the closest one to the initial estimation.

The above ambiguity disappears if the EAOM is applied with its inherent constrains. To start with, the single-parameter version of the EAOM, Eq. (16), is adapted to account for the two different anions occurring in the coordination sphere—the oxygen and sulfur:

$$B_{kq} = B_{kq}^{res} + \tilde{W}_{kq}^{O}\tilde{e}^{O} + \tilde{W}_{kq}^{S}\tilde{e}^{S} \tag{21}$$

with coefficients W given by Eq. (19), B_{kq}^{res} and the remaining data taken from Ref. 19. It turns out that this simplest version of the EAOM, with only two effective parameters $\tilde{e}^{O}$ and $\tilde{e}^{S}$, describes fairly well the three electronic INS transitions:[45,55] 74 meV $[\Gamma^5(1)\rightarrow\Gamma^3]$, 83 meV $[\Gamma^5(1)\rightarrow\Gamma^4]$, and 87 meV $[\Gamma^5(1)\rightarrow\Gamma^5(2)]$. These intervals can be easily matched by a slight refining of the *ab inito* ratios $s_{\pi\sigma}$. Figure 5(c) shows the resulting energies and the transition probabilities estimated in terms of the squares of the matrix elements of the Zeeman operator between the initial and final states.[56] The Debye-Waller and 5*f*-electron form factors are not taken into account since we are interested only in comparison of various numerical simulations without a direct reference to the experimental recordings. The Gaussian shape of the figured transitions has only an illustrative character. The present simulation of the INS transitions does not differ much from the previous one shown in Fig. 5(b).[19] Taking into account a finite width of the experimental lines and limited range of the measurable energies both the simulations seem acceptable. In particular, the main lines around 80 meV are quite similar to the measured ones.[45,55] The line at about 40 meV was neither observed nor excluded by the experimental data since it is relatively weak and lies in the region of the phonon sidebands. Further INS investigations with higher incident neutron energies could decisively verify the predicted positions of the Γ^2 and $\Gamma^{1(2)}$ levels. The ordered magnetic moment of $2.11\mu_B$ as determined from the obtained wave functions, is higher than the observed one of $2.00\mu_B$.[54] Nevertheless it can be reduced to about $2.04\mu_B$ due to the overlap and covalency effects.[57] Our phenomenological results can be compared with *ab inito* predictions. The parameter $\tilde{e}^{O}=370.2$ meV is about 10% higher than the theoretical value of e_σ from Table II, whereas $\tilde{e}^{S}=157.1$ meV is lower than its counterpart. The differences between the corresponding phenomenological and theoretical parameters become even more pronounced in the case of the corresponding B_{kq} parameters listed in Table III. Taking into account inherent limitations of the *ab inito* calculations due to numerous approximations and uncertainty of the Sternheimer shielding factors and dipole and quadrupole polarizabilities, such a divergence seems inevitable. Nevertheless, we still propose to keep the ratios of the theoretical values of the EAOM parameters [Eqs. (8) and (17)] in our simplified phenomenological models [Eqs. (16) and (18)] assuming them to be more reliable than the theoretical EAOM parameters themselves because of the restricted number of contributions they are dependent

TABLE III. Comparison of various B_{kq} sets obtained for UOS (in meV).

	B_{20}	B_{40}	B_{44}	B_{60}	B_{64}
Ab initio calculations	−180	−545	−119	424	104
AOM	−117	−567	−11	632	250
Model from Ref. 19	−147	−579	−39	595	447
EAOM	−159	−624	−21	627	380

on an expected partial cancellation of the calculation errors.

The B_{kq} parameters determined within the EAOM approach lie between those obtained using the conventional AOM and the refined model from Ref. 19. The phenomenological sets do not differ much, especially these in the two last lines of Table III. The *ab initio* values look less satisfactory, especially the nonaxial B_{k4} ($k=4,6$) parameters. The outstanding discrepancy of the latter can be attributed to the competing contributions of the oxygen and chalcogenide groups resulting in relatively small values of these parameters and increased cumulative relative errors.[19]

The low-symmetry crystals UX_2 considered in Sec. III B may serve as the next example of application of the EAOM. The model allows one to reduce 15 (US_2,USe_2) or nine (UTe_2) B_{kq} parameters specific for the point group symmetries in these compounds to only 1–3 EAOM parameters. Note that very construction of any version of the EAOM, including the single-parameter one Eq. (18), ensures accuracy of the electronic structure simulation not worse than that obtained from the *ab initio* calculations. This is because the *ab initio* calculations determine not only the starting values of the parameters but also the coefficients W and residual off-AOM terms in Eqs. (16) and (18). Thus, with the EAOM one can try to reproduce the electronic structure of any compound even if the available experimental data are limited merely to a single thermodynamic characteristic like the magnetic susceptibility discussed in Sec. III B. In the specific case of UX_2, the theoretical curves displayed in Fig. 1 represent simultaneously the initial phenomenological dependencies in our model. The corresponding EAOM parameters listed in Table II are thus the natural and right starting values in subsequent steps of the further interpretation of the electronic structure and the forthcoming experimental data.

V. CONCLUDING REMARKS

The crystal field potential in the quasiphenomenological enhanced angular overlap model proposed here is divided into two parts: the main part, adjustable, which comprises the contributions amenable to the conventional AOM parametrization, and the residual one, fixed, representing all the remaining terms. The fixed, off-AOM residual part contains the electrostatic contributions of further neighbors and the ligand polarization contribution, the accuracy of determination of which hinges on the available ionic polarizabilities and the shielding factors. Much more complicated renormalization terms in the CF potential are handled in the phenomenological way together with the core, charge penetration, and interionic exchange contributions. The parametrization applied is known from the usual AOM approach. Its simplicity is a consequence of the axial local symmetry of the encoded contributions and their additivity.

The aptness of such a discrimination between the contributions is illustrated by an increasing amount of examples of first-principles calculations in the literature and also by the results presented in this paper. Additionally, the calculations provide the ratios of the intrinsic parameters that may be employed in further applications of EAOM. The simulations performed for the virtual UX_2 crystal of CaF_2 symmetry give an idea about dependence of the EAOM parameters on metal-ligand distance. They show the evolution of the mutual relations between the AOM-consistent contributions. The observed behavior of the AOM-consistent contributions to the intrinsic parameters in the limit of the shortest metal-ligand distances touches a more complex problem of the CF effect in metallic systems. A comparison of these simulations with the *ab initio* calculations for the actual UX_2 compounds evidences a certain volatility of the intrinsic parameters. It turns out that the assumption, commonly accepted for models based on the superposition anzatz (conventional AOM or SPM and their various modifications), saying that the intrinsic parameters are smooth functions of the metal-ligand distance, is not always valid due to the various Madelung energies of the ions in real crystals and a high sensitivity of the intrinsic parameters to these energies. This points to the necessity of enforcing each particular implementation of the phenomenological model with the *ab initio* calculations for an actual specimen just as is postulated in the EAOM.

The EAOM ensures a highly compact description of the electronic structure of even such complex ionic systems as the actinide crystals. The examples discussed in the paper represent various kinds of conceivable applications. The case of experimental data limited to only certain magnetic characteristics of systems of low crystal symmetries is illustrated for the UX_2 series. In another example, the electronic structure for NpOX is predicted by transforming the intrinsic parameters for the corresponding UOX compounds and exploiting relations between the parameters calculated *ab initio*. Various experimental data are available in the case of UOS. They include magnetic and thermodynamic properties as well as the inelastic neutron scattering spectra. Nevertheless, the electronic structure cannot be resolved within the conventional CF parametrization scheme without additional assumptions of rather heuristic nature. The EAOM is shown to be capable of describing of all of the observed properties unequivocally.

The EAOM is open for further improvements. We mention here a more accurate potential that could be obtained from lattice self-consistent calculations[4,10] to correct the zero-order wave functions used in the calculations. Direct evaluation of multipole polarizabilities and shielding factors for a given specimen may be important for calculations of the residual part of the crystal field, since these quantities depend on the Madelung energies of the ions.[36] Perhaps the analogous idea of partitioning of the CF potential into phenomenological and fixed parts may also be applied to much more complicated metallic systems.

ACKNOWLEDGMENTS

The author thanks Professor Robert Troć (ILT&SR, Wrocław) for providing the source recordings of the susceptibility data for UX_2, Dr. Michael F. Reid (University of Canterbury, Christchurch, New Zealand) for the *f*-shell programs, Dr. Michelle Faucher (Clamart, France) for the CHLOE program, and Professor Jacek Mulak (ILT&SR, Wrocław) for careful and critical reading of the manuscript.

APPENDIX A

The parametric Hamiltonian[10,23,58] contains a free-ion, spherically symmetric part H_0 and crystal field potential V,

$$H = H_0 + \sum_i V(\mathbf{r}_i/r_i), \tag{A1}$$

where the summation index i runs over all f electrons. The free-ion part can be written as follows:

$$H_0 = E_{av} + \sum_{k=2,4,6} F^k(nf,nf) f_k + \zeta_{5f} A_{S0} \alpha L(L+1) + \beta G(G_2) + \gamma G(R_7) + \sum_{k=0,2,4} M^j m_j + \sum_{k=2,4,6} P^k p_k \tag{A2}$$

where E_{ave} is the spherically symmetric one-electron part of the Hamiltonian, $F^k(nf,nf)$ and ζ_{5f} represent the radial integrals due to the electrostatic and spin-orbit interactions, while f_k and A_{SO} are the angular operators corresponding to these interactions, respectively. The α, β, and γ parameters are associated with the two-body correction terms. $G(\mathrm{G}_2)$ and $G(\mathrm{R}_7)$ are Casimir operators for the G_2 and R_7 groups and L is the total orbital angular momentum. The electrostatically correlated spin-orbit perturbation is represented by the P_k parameters and those of the spin-spin and spin–other-orbit relativistic corrections by the M_j parameters. The operators associated with these parameters are designated by m_j and p_k, respectively.

APPENDIX B

The main contributions to the one-electron CF potential in nonmetallic crystals are listed here. For derivations and a detailed discussion see Ref. 10. Some numerical questions related to multicenter integrals and summation of weakly convergent infinite series are dealt with in Refs. 11, 14, and 29.

From definition, the AOM-consistent part of the CF potential and thus the AOM-consistent contributions in Eqs. (13) and (14) are partitioned due to ligands according to Eq. (3). Therefore, without loss of generality we can consider only a single ligand potential v_t in the local coordinates centered at the metal site, the z axis of which is directed toward the ligand. Due to the axial symmetry of the ligand potential the orientation of the x and y axes is immaterial. Atomic units are applied throughout this section.

$$v_t^{pcm}(\mathbf{r}) = \frac{2}{|\mathbf{r} - \mathbf{R}_t|} \tag{B1}$$

$$v_t^{cp}(\mathbf{r}) = \sum_\tau \left[\hat{J}(\chi_{t\tau}(\mathbf{r}), \chi_{t\tau}(\mathbf{r})) - \frac{8}{|\mathbf{r} - \mathbf{R}_t|} \right], \tag{B2}$$

$$v_t^{ex}(\mathbf{r}) = -\sum_\tau \hat{K}(\chi_{t\tau}(\mathbf{r}), \chi_{t\tau}(\mathbf{r})), \tag{B3}$$

$$v_t^{ov} = \sum_\tau |\chi_{t\tau}\rangle\langle\chi_{t\tau}| \Big\{ \langle\varphi|\hat{h}_0|\varphi\rangle - 2\hat{h}_0 + \sum_{t',\tau'} [\hat{h}_0 - \hat{J}(\varphi,\varphi)] |\chi_{t'\tau'}\rangle \times \langle\chi_{t'\tau'}| \Big\}, \tag{B4}$$

$$v_t^{cs} = \sum_\nu \sum_\tau \Bigg(|\langle\xi_\nu|\chi_{t\tau}\rangle|^2 [2\hat{J}(\xi_\nu,\xi_\nu) - \hat{K}(\xi_\nu,\xi_\nu)] - 2\langle\xi_\nu|\chi_{t\tau}\rangle \times [2\hat{J}(\chi_{t\tau},\xi_\nu) - \hat{K}(\chi_{t\tau},\xi_\nu)] + \sum_{\substack{t',\tau' \\ t' \neq t}} \langle\xi_\nu|\chi_{t\tau}\rangle\langle\chi_{t'\tau'}|\xi_\nu\rangle \times [2\hat{J}(\chi_{t\tau},\chi_{t'\tau'}) - \hat{K}(\chi_{t\tau},\chi_{t'\tau'})] \Bigg), \tag{B5}$$

$$v_t^{cov} = \sum_\tau \frac{\tilde{h}_{t\tau}|\chi_{t\tau}\rangle\langle\chi_{t\tau}|\tilde{h}_{t\tau}}{\Delta_{t\tau}}. \tag{B6}$$

φ_m and ξ_ν in the above equations denote the $5f$ and $6s,6p$ orbitals of the metal ion obtained from the Dirac-Slater calculations for the free ion, $\chi_{t\tau}$ stand for the analogous ns and np orbitals of the anion and m,ν,τ are the corresponding sets of quantum numbers. $\hat{J}$ and $\hat{K}$ are the usual Coulomb direct and exchange operators (see for instance Ref. 10),

$$\hat{h}_0 = \frac{-\nabla^2}{2} + v_0^M + \sum_t v_{0t}^L + V^{fn}, \tag{B7}$$

where v_0^M and v_{0t}^L are the Dirac-Slater free-ion metal and ligand potentials.

$$\tilde{h}_{t\tau} = h_{t\tau} - \sum_{t'\tau'} \sum_{t'',\tau''} |\chi_{t'\tau'}\rangle\langle\chi_{t'\tau'}|h_{t\tau}|\chi_{t''\tau''}\rangle\langle\chi_{t''}|, \tag{B8}$$

$$h_{t\tau} = h_0 - \hat{J}(\chi_{t\tau},\chi_{t\tau}), \tag{B9}$$

$$\Delta_{t\tau} = \langle\varphi|h_{t\tau}|\varphi\rangle - \langle\chi_{t\tau}|h_0|\chi_{t\tau}\rangle. \tag{B10}$$

$v_t^{pcm}(\mathbf{r})$ represents only ligands as point charges (monopoles).

The remaining contributions are conveniently presented as a part of the electrostatic model, which includes all ions in the crystal represented by a sequence of point monopole, dipole, quadrupole, etc.:

$$V^{el} = V^{nn\ pol} + V^{fn} + V^{pcm}. \tag{B11}$$

Note that the two first terms on the right-hand side of Eq. (B11) are part of V^{res} in Eq. (15), whereas the third term enters into V^{pr} in Eq. (13). The electrostatic potential V^{el} of point multipoles can be expanded in series of spherical harmonics, similarly to the global CF potential in Eq. (1). The corresponding contribution to the B_{kq} parameters has the following form:[10]

$$B_{kq}^{el} = \langle r^k\rangle \sum_t \sum_n \sum_\mu (-1)^{k+q+\mu} \left[\frac{(2k+2n+1)!}{2^n(2k)!} \right]^{1/2} \times \begin{pmatrix} k & n & k+n \\ q & \mu & -q-\mu \end{pmatrix} \frac{1}{R^{k+n+1}} M_{t\mu}^{(n)} C_{q+\mu}^{(k+n)}(\mathbf{R}_t/R_t), \tag{B12}$$

where $\langle r^k\rangle$ is the mean value of r^k for the $5f$ orbital. $\mathbf{M}_t^{(n)}$ is

the $2n$-pole electric momentum induced on ion t, where t runs over all the ions in the infinite net and μ runs over the components of $\mathbf{M}_t^{(n)}$. The state of electrostatic equilibrium between the $\mathbf{M}_t^{(n)}$ moment and the remaining multipole moments of the crystal lattice is represented by the following equations determining the electric multipole moments $\mathbf{M}_t^{(n)}$:[10,14]

$$\mathbf{M}_t^{(n)} = \sum_{t'} \sum_{p=0,1,2} (-1)^{n+1} \alpha_t^{(n)} \mathbf{I}^{(2n)} \boldsymbol{\nabla}_{t'}^{(n)} \left[\mathbf{M}_{t'}^{(p)} \cdot \boldsymbol{\nabla}_{t'}^{(p)} \frac{1}{\mathbf{R}_{t'}} \right] \tag{B13}$$

where $\mathbf{I}^{(2n)}$ is the diagonal unit tensor of rank $2n$. $\alpha_t^{(n)}$ is the $2n$-pole polarizability.

APPENDIX C

The temperature dependence of the paramagnetic susceptibility is given by the Van Vleck formula[59]

$$\chi_\alpha(T) = \frac{N_A \mu_B^2}{Z} \sum_\gamma (\beta a_{\gamma,\alpha} + 2 b_{\gamma,\alpha}) \exp(-\beta E_\gamma) \tag{C1}$$

with

$$a_{\gamma,\alpha} = \sum_{\substack{\gamma' \\ E_{\gamma'} = E_\gamma}} |\langle \gamma | L_\alpha + g S_\alpha | \gamma' \rangle|, \tag{C2}$$

$$b_{\gamma,\alpha} = \sum_{\substack{\gamma' \\ E_{\gamma'} \neq E_\gamma}} \frac{|\langle \gamma | L_\alpha + g S_\alpha | \gamma' \rangle|}{E_{\gamma'} - E_\gamma}, \tag{C3}$$

$$Z = \sum_\gamma \exp(-\beta E_\gamma). \tag{C4}$$

$\beta = 1/kT$, $\alpha = x, y, z$, the index γ numbers the eigenstates, the E_γ's denote their energies, L_α and S_α are the α components of the total orbital and spin operators, and g is the gyromagnetic ratio of the electron spin.

*Email address: gajek@int.pan.wroc.pl

[1] H. A. Bethe, Ann. Phys. **3**, 135 (1929).
[2] C. K. Jorgensen, R. Pappalardo, and H. H. Schmidtke, J. Chem. Phys. **39**, 401 (1963).
[3] C. E. Schäffer and C. K. Jorgensen, Mol. Phys. **9**, 401 (1965).
[4] M. Gerloch, J. H. Harding, and G. Wooley, Struct. Bonding (Berlin) **46**, 1 (1981).
[5] Z. Gajek and J. Mulak, J. Phys.: Condens. Matter **4**, 427 (1992).
[6] D. J. Newman, Adv. Phys. **20**, 197 (1971).
[7] W. Kohn and L. J. Sham, Phys. Rev. A **140**, 1133 (1965).
[8] M. Fähnle, J. Magn. Magn. Mater. **151**, L5 (1995).
[9] K. N. Kudin, G. E. Scuseria, and R. L. Martin, Phys. Rev. Lett. **89**, 266402 (2002), and references therein.
[10] J. Mulak and Z. Gajek, *The Effective Crystal Field Potential* (Elsevier, Amsterdam, 2000).
[11] Z. Gajek, J. Mulak, and M. Faucher, J. Phys. Chem. Solids **48**, 947 (1987).
[12] S. Sugano and R. G. Schulman, Phys. Rev. **130**, 517 (1967).
[13] *Crystal Field Handbook*, edited by D. J. Newman and B. K. C. Ng (Cambridge University Press, Cambridge, U.K., 2000).
[14] M. Faucher and D. Garcia, Phys. Rev. B **26**, 5451 (1982).
[15] P. M. Levy and S. Zhang, Phys. Rev. Lett. **62**, 78 (1989).
[16] I. A. Garifullin, T. O. Farzan, G. G. Khaliullin, and E. F. Kukovitsky, J. Phys. F: Met. Phys. **15**, 979 (1985).
[17] C. Brouder, http://arxiv.org/list/cond-mat/0308058.
[18] D. J. Newman and B. Ng, J. Phys. C **19**, 389 (1986).
[19] Z. Gajek, J. Phys.: Condens. Matter **12**, 415 (2000).
[20] Z. Gajek, J. Magn. Magn. Mater. **272–276**, e415 (2004).
[21] R. McWeeny and B. T. Sutcliffe, *Methods of Molecular Quantum Mechanics* (Academic Press, New York, 1969).
[22] R. E. Watson, Phys. Rev. **111**, 1108 (1958).
[23] B. G. Wybourne, *Spectroscopic Properties of Rare Earths* (Interscience, New York, 1965), Chap. 7.
[24] C. E. Schäffer, Struct. Bonding (Berlin) **5**, 68 (1968).
[25] A. R. Edmonds, *Angular Momentum in Quantum Mechanics* (Princeton University Press, Princeton, NJ, 1957).
[26] M. Rotenberg, R. Bivins, N. Metropolis, and J. K. Wooten, *The 3-j and 6-j Symbols* (MIT Press, Cambridge, MA, 1959).
[27] M. Faucher, D. Garcia, and C. Jorgensen, Chem. Phys. Lett. **129**, 387 (1986).
[28] W. H. Kleiner, J. Chem. Phys. **20**, 1784 (1952).
[29] Z. Gajek and J. Mulak, Int. J. Quantum Chem. **28**, 889 (1985).
[30] N. Sato, H. Masuda, M. Wakeshima, K. Yamada, and T. J. Fujino, J. Alloys Compd. **265**, 115 (1998).
[31] K. Stowe, J. Solid State Chem. **127**, 202 (1996).
[32] H. Noël, M. Potel, R. Troć, and L. Shlyk, J. Solid State Chem. **126**, 22 (1996).
[33] D. D. Koeling and B. N. Harmon, J. Phys. C **10**, 3107 (1977).
[34] D. D. Koeling, Computer code *ATOM*, 1980, a derivative of the Liberman-Waber-Cromer code Phys. Rev. **137** A27 (1965)].
[35] M. Faucher (private communication).
[36] P. C. Schmidt, A. Weiss, and T. P. Das, Phys. Rev. B **19**, 5525 (1979).
[37] R. M. Sternheimer, M. Blume, and R. F. Peierls, Phys. Rev. **173**, 376 (1968).
[38] P. Erdös and J. Robinson, *The Physics of Actinide Compounds* (Plenum Press, New York, 1983).
[39] Z. Gajek (unpublished).
[40] W. T. Carnall and H. M. Crosswhite, Argonne National Laboratory Technical Report No. ANL-84/90, 1985 (unpublished).
[41] Z. Gajek, J. C. Krupa, and E. Antic-Fidancev, J. Phys.: Condens. Matter **6**, 557 (1997).
[42] M. Reid (private communication); in *Crystal Field Handbook* (Ref. 13), see also Appendix C, p. 254.
[43] Z. Gajek, M. P. Lahalle, J. C. Krupa, and J. Mulak, J. Less-Common Met. **124**, 351 (1988).
[44] R. Osborn, A. D. Taylor, Z. Bowden, M. A. Hackett, W. Hayes, M. T. Hutchings, G. Amoretti, R. Caciuffo, A. Blaise, and J. M. Furnier, J. Phys. C **21**, L931 (1988).
[45] G. Amoretti, A. Blaise, M. Bonnet, R. Caciuffo, P. Erdös, H.

Noël, and P. Santini, J. Magn. Magn. Mater. **139**, 339 (1995).
[46] L. Shlyk, R. Troć, and D. Kaczorowski, J. Magn. Magn. Mater. **140–144**, 1435 (1995).
[47] H. Noël and R. Troć, J. Solid State Chem. **126**, 22 (1996).
[48] C. Rudowicz and J. Qin, J. Lumin. **110**, 39 (2004).
[49] C. Rudowicz and J. Qin, J. Alloys Compd. **385**, 238 (2004).
[50] There is no unique set of the B_{kq} parameters in the case of low-symmetry systems. Although the parameters presented in the paper are strictly defined in the crystallographic coordination system, they have to be standardized before they are compared with other data. For further details see Refs. 10, 60–62, and the references therein.
[51] Y. R. Shen and W. B. Holzapfel, J. Phys.: Condens. Matter **6**, 2367 (1994).
[52] Y. Shen and K. L. Bray, Phys. Rev. B **58**, 5305 (1998).
[53] G. Amoretti, A. Blaise, J. M. Collard, R. O. A. Hall, M. J. Mortimer, and R. Troć, J. Magn. Magn. Mater. **46**, 57 (1984).
[54] R. Troć, Inorg. Chim. Acta **140**, 67 (1987).
[55] G. Amoretti, A. Blaise, R. Furnier, J. M. Larroque, and R. Osborn, J. Phys.: Condens. Matter **1**, 5711 (1989).
[56] R. J. Birgeneau, J. Phys. Chem. Solids **102**, 1141 (1972).
[57] Z. Gajek and J. Mulak, J. Magn. Magn. Mater. **53**, 63 (1985).
[58] G. K. Liu, in *Crystal Field Handbook* (Ref. 13), p. 65.
[59] J. H. V. Vleck, *The Theory of Electric and Magnetic Susceptibilities* (Oxford University Press, Oxford, 1932).
[60] Y. Y. Yeung, in *Crystal Field Handbook* (Ref. 13), p. 160.
[61] C. Rudowicz and J. Qin, Phys. Rev. B **67**, 174420 (2003).
[62] G. W. Budrick and M. F. Reid, Mol. Phys. **33**, 59 (2004).